Spectrochimica Acta Part B 87 (2013) 121–129

Contents lists available at ScienceDirect

Spectrochimica Acta Part B

journal homepage: www.elsevier.com/locate/sab

Molecular formation dynamics of 5-nitro-2,4-dihydro-3H-1,2,4-triazol-3-one, 1,3,5-trinitroperhydro-1,3,5-triazine, and 2,4,6-trinitrotoluene in air, nitrogen, and argon atmospheres studied using femtosecond laser induced breakdown spectroscopy

Sunku Sreedhar, E. Nageswara Rao, G. Manoj Kumar *, Surya P. Tewari, S. Venugopal Rao *

Advanced Centre of Research in High Energy Materials (ACRHEM), University of Hyderabad, Prof. C. R. Rao Road, Gachibowli, Hyderabad 500046, India

ARTICLE INFO

Article history:
Received 30 November 2012
Accepted 12 May 2013
Available online 20 May 2013

Keywords:
Femtosecond LIBS
Explosives detection
Molecular CN
Temporal dynamics

ABSTRACT

Femtosecond laser induced breakdown spectroscopic (LIBS) studies were performed on three high energy materials namely 5-nitro-2,4-dihydro-3H-1,2,4-triazol-3-one (NTO), 1,3,5-trinitroperhydro-1,3,5-triazine (RDX), and 2,4,6-trinitrotoluene (TNT). LIBS spectral features were obtained for these samples in three different atmospheres i.e. air, nitrogen, and argon. Different molecular to elemental ratios in these three atmospheres were investigated in detail. CN/C and CN/N ratios were observed to be prominent in nitrogen and air atmospheres. We attempt to elucidate the role of several reactions involving CN molecular formation in connection with discrepancies obtained in the measured ratios. The complete temporal dynamics of atomic C (247.82 nm) and CN (388.20 nm) molecular species in three different atmospheres are elaborated. The decay rates of C peak were found to be longest (96 ns–121 ns) in argon atmosphere for all the samples. The decay rates of CN peak (388.2 nm) were longer (161 ns–364 ns) in nitrogen compared to air and argon atmospheres. We also attempt to explicate the decay mechanisms with respect to the molecular species formation dynamics in different atmospheres.

1. Introduction

Laser induced breakdown spectroscopy (LIBS) has recently been established as a successful analytical tool for elemental analysis [1,2]. There is growing interest for this technique in diverse fields of research because of its unique advantages such as simultaneous single shot measurement and multi-elemental detection capabilities. This technique has been successfully utilized in diverse fields such as pharmaceuticals [3,4], archeology [5], materials science [6], biology [7] and explosives detection [8–11]. Especially, the standoff detection potential makes this technique an attractive contrivance for detection of high energy materials (HEMs). Among recent successful reports Gottfried et al. demonstrated field-tested standoff LIBS for identification of chemical and biological threats [8] and reviewed the challenges lying ahead for detection of explosive residue materials [9]. Abdelhamid et al. analyzed several explosive residues on glass surface successfully using optical catapulting in combination with LIBS [10]. Trace level detection of several explosives on Al substrate was performed by Lazic and co-workers [11]. The use of femtosecond (fs) laser as an excitation source has been shown to offer several advantages. In comparison to ns LIBS, fs laser produced plasma has negligible interaction with the input pulses [12–14]. This implies that most of the pulse energy is utilized in creating plasma resulting in small, deep crater formation and thereby precise, smooth structures in solid targets [12]. Furthermore, the produced plasma emits nearly background-free spectra devoid of continuum [13]. The shorter pulse duration and higher peak intensity associated with fs laser pulses enrich the capabilities of fs LIBS technique such as minimized energy dissipation in the sample resulting in lower ablation thresholds, effective ablation due to energy confinement, minimal sample heating and collateral damage, higher shot-to-shot stability and the possibility of beam filamentation over a period of few kilometers for implementing remote LIBS [13–15]. Several groups have investigated LIBS with fs laser pulses for identification of biological samples/bacteria [15–17], animal tissue studies [18], graphite analysis [19], monitoring of cultural heritage [20], and studies on HEMs [21,22] etc. Baudelet et al. [16] explored the possibilities of bacterial detection with both ns and fs LIBS and made a comparative study. Recently fs LIBS technique was employed for combustion diagnostics and demonstrated that this can be a useful tool for in-situ determination and local mapping of fuel content in hydrocarbon–air combustible mixtures [23]. Fs LIBS has tremendous potential and is evidenced by the fact that recent studies including a variety of materials such as reactor fuel coated particles [24], uranium [25], and electrode/electrolyte interfaces [26] etc. have been successfully demonstrated. The usage of fs pulses in other

* Corresponding authors.
E-mail addresses: manojsp@uohyd.ernet.in (G. Manoj Kumar), svrsp@uohyd.ernet.in (S. Venugopal Rao).

0584-8547/$ – see front matter © 2013 Elsevier B.V. All rights reserved.
http://dx.doi.org/10.1016/j.sab.2013.05.006

important technological fields, for instance micromachining, is well understood and established [27]. Ultrafast laser pulses possess large spectral bandwidth and there are several parameters of these laser pulses that can affect the plasma extensive investigation of the plasma properties with changing bandwidth [28], pulse chirp [29] and input energy [30] were carried out.

Materials such as plastics, organic explosives and also few bacterial samples possessing composition of the type "$C_\alpha H_\beta N_\gamma O_\delta$" exhibit similar molecular and elemental signatures in their LIBS spectra. These molecular peaks are important and are used widely for classification of these materials among others. Statistical techniques have been utilized by many groups to classify several explosive samples using molecular and atomic peaks [31–34]. Molecular emission has also been extensively used for the materials such as plastics due to their complex composition. Spatial and temporal distributions of CN and C_2 emissions from polymers have been studied in detail [35]. The usage of molecular emission to calculate plasma temperature from graphite samples has been reported recently. The temporal and spatial evolutions of the CN and C_2 emissions from graphite and some polymers have been studied with ns laser produced plasmas [36–43]. Harilal et al. [37] studied the formation of graphite plasma in helium gas and air with ns laser pulses and in nitrogen with fs laser pulses [38]. Dong et al. have investigated laser ablation of coal sample in air, argon and helium atmospheres with time resolved ns LIBS [44]. Dagdigian's group [45–47] performed extensive simulations and experiments on organic materials and explained, through reaction kinetics, the formation of molecular species within ns plasma. Temporal features of the molecular peaks of some HEMs [48] and few nitro compounds [49] were studied in air and argon environment using ns LIBS technique. Mainly there are three possibilities which give rise to the formation of CN molecular formation in plasma [34]. One possibility is the direct evaporation of molecular radicals present in the sample during the process of breakdown, second possibility is that it can be formed due to the secondary reactions occurring between C, N and C_2 present in the plasma, and third one is that there may be a reaction between C and C_2 from the plasma with atmospheric Nitrogen leading to the formation of CN radical. Our previous work explained the CN molecular formation dynamics in plasma created in different HEMs (recorded in ambient air) using fs and ns pulses. Our results emphasized that the CN molecular peak intensity was higher in fs LIBS data contrasted with ns LIBS data. The ratio of CN/C was observed stronger in fs LIBS spectra compared to ns LIBS spectra [50]. Few studies are available in literature explaining the formation dynamics of CN species of plastics and graphite with ns produced plasma. Grégoire et al. explained the spatial distribution of CN, C, and N species for various plastic materials [35]. Furthermore, very few studies reported in literature tried explaining the temporal dynamics of HEMs with ns pulses. Babushok et al. [47] presented a modeling of RDX LIBS plasma using several possible reactions occurring within the plasma. Sovova et al. [48] presented temporal features of CN, C_2 and C emission of four explosives in air and argon environments. To the best of our knowledge there are no reports till date to explain the temporal dynamics of HEMs recorded using fs pulses. The present study aims to investigate the molecular features of LIBS spectra recorded for the samples of NTO, RDX and TNT in three environments viz. air, nitrogen, and argon utilizing fs laser pulses.

Plasma chemistry involves the formation of molecular fragments which is a complex phenomenon. The surroundings of plasma influence the molecular formation significantly. Therefore, it is imperative to identify the sources for formation of CN and C_2 molecules, since this data could be of significant help in classification. We had chosen three different purge gases: nitrogen (implying 100% nitrogen), ambient air (approximately 75% nitrogen) and argon (0% nitrogen). Argon purging enabled the study of CN molecular species formation resulting solely from the sample constituents (C and N). We attempt to understand the CN molecular formation mechanism and figure out the contribution from surrounding atmosphere to the plasma. Experiments were performed in a controlled manner such that purging the gas on to the sample exactly where the plasma was formed. The spectral features obtained with three different atmospheres are explained with the help of molecular/elemental and elemental/elemental peak ratios. The temporal variation of the molecular emission (CN) was also studied. The investigation of spectral features of these HEMs in nitrogen, air and argon environments using fs LIBS is being presented extensively.

2. Experimental setup

Amplified Ti:sapphire laser pulses with duration of ~40 fs, maximum energy of 2.5 mJ delivered at a repetition rate of 1 kHz (central wavelength of 800 nm) were used in all the experiments [50]. The fs laser pulses were focused on the target sample with 8 cm plano-convex lens. The energy used to produce plasma was ~1.2 mJ and corresponding fluence estimated was ~22 J/cm^2. Dense plasma was formed at the focal region. A collection lens system unit was placed to collect the light from plasma and light passed through a fiber optic cable and finally transferred to a gated ICCD spectrometer (Andor i-star DH734 ICCD + ME 5000 Mechelle spectrograph, resolution 5000). The complete details of experimental setup were presented in our previous work [50]. The sample powder was ground with an agate motor and the resulting powder was pelletized using a hydraulic press under a base pressure of 8–10 t. The pellets thickness was estimated to be ~2–3 mm. The samples were translated using motorized stages (for independent measurements) and manually (for time-resolved measurements) such that laser pulses hit a fresh target/sample region every time. Argon and nitrogen gases were purged through nozzle onto the sample where laser was focused onto the pellets. We ensured that there was no interference from atmosphere while purging with nitrogen and argon gases. We recorded the LIBS spectra of air, argon, and nitrogen independently and the spectra confirmed the absence of oxygen peaks in nitrogen and argon atmospheres. Three HEMs samples NTO (5-nitro-2,4-dihydro-3H-1,2,4-triazol-3-one; $C_2H_2N_4O_3$), RDX (1,3,5-trinitroperhydro-1,3,5-triazine; $C_3H_6N_6O_6$), and TNT (2,4,6-trinitrotoluene; $C_7H_5N_3O_6$) were used in our studies for investigation of molecular emission with fs LIBS. All samples have same elements C, H, N and O with different composition. The spectral emission from LIBS plasma offered similar peaks with different magnitudes. The structure and composition of three samples are presented in Table 1.

3. Results and discussion

3.1. Spectral analysis

Fig. 1(a) [spectral range of 240–520 nm] and (b) [spectral range of 630–880 nm] illustrates the spectra obtained using fs pulses for NTO sample. In each case the top graph corresponds to the LIBS spectra obtained in air whereas the second one in nitrogen atmosphere and

Table 1
Compositional and structural information of HEMs.

Sample	Composition	Nitro-groups	C/N	C/O	O/N	H/N	Structure
NTO	$C_2H_2N_4O_3$	1	0.5	0.6	0.75	0.5	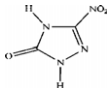
RDX	$C_3H_6N_6O_6$	3	0.5	0.5	1	1	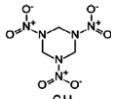
TNT	$C_7H_5N_3O_6$	3	2.3	1.16	2	1.6	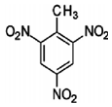

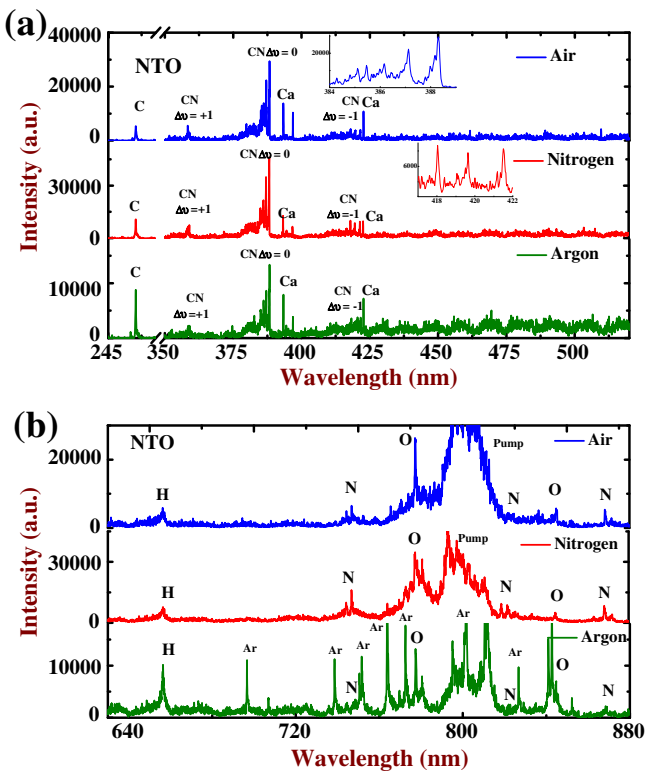

Fig. 1. LIBS spectra of NTO obtained with fs laser excitation in three different atmospheres. A gate width of 800 ns and 100 ns initial delay were utilized to record the spectra. (a) Spectral features in the 240 nm–520 nm range and (b) spectral features in the 630 nm–880 nm spectral range.

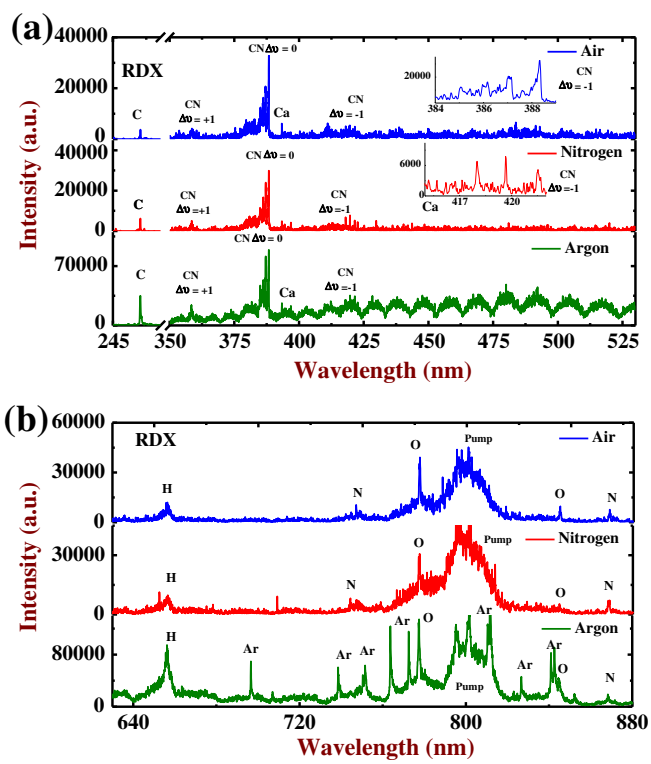

Fig. 2. LIBS spectra of RDX obtained with fs laser excitation in three different atmospheres. The gate width of 800 ns and 100 ns initial delay were utilized to record the spectra. (a) Spectral features in the 240 nm–520 nm range and (b) spectral features in the 630 nm–880 nm spectral range.

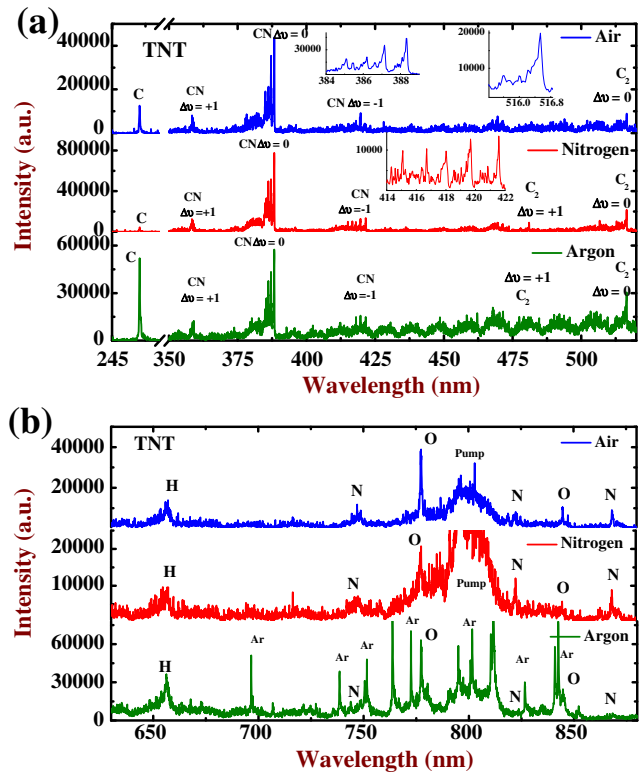

Fig. 3. LIBS spectra of TNT obtained with fs laser excitation in three different atmospheres. The gate width of 800 ns and 100 ns initial delay were utilized to record the spectra. (a) Spectral features in the 240 nm–520 nm range and (b) spectral features in the 630 nm–880 nm spectral range.

the final spectra was obtained in argon atmosphere. Each single spectrum was the resultant of accumulation of 500 laser shots. Similarly, spectra depicted in Fig. 2(a) and (b) correspond to RDX sample in the aforesaid three atmospheres. Fig. 3(a) and (b) corresponds to data obtained from TNT sample. The spectral peaks corresponding to a particular atom/molecular species have been assigned and are summarized in the graphs. Elemental peaks corresponding to C-247.82 nm, N-821.50 nm, 822.35 nm, 867.80 nm, 868.80 nm, O-777.2, 844.55 nm and H-656.2 nm lines were clearly observed in the spectra. We have also observed the violet band transitions of CN molecule in three different regions. These CN violet band lines corresponding to $B^2S_u^+ - X^2S_g^+$ states with transitions $\Delta\nu = 0$ were observed at 388.28 nm ($\nu' - \nu''$) (0–0), 387.07 nm (1–1), 386.16 nm (2–2), 385.40 nm (3–3) and 385.01 nm (4–4), transitions with $\Delta\nu = +1$ were observed at 421.50 nm ($\nu' - \nu''$) (0–1), 419.63 nm (1–2), 418.03 nm (2–3), 416.78 nm (3–4) and 415.81 nm (4–5) and transition with $\Delta\nu = -1$ was observed at 359.02 nm ($\nu' - \nu''$) (1–0) regions. C_2 swan bands corresponding to states $D^3\Pi_g - A^3\Pi_u$ with transitions $\Delta\nu = 0$ were observed at 516.47 nm ($\nu' - \nu''$) (0–0) and transitions with $\Delta\nu = -1$ were observed at 473.63 nm ($\nu' - \nu''$) (1–0), 471.63 nm (2–1) and 469.70 nm (3–1) regions. However, all the elemental and molecular features observed for three samples in three atmospheres were slightly dissimilar. Depending on the sample nature as well as surrounding atmosphere, slight variations (in intensities that were calculated using simply the peak heights) were observed. Table 2 summarizes all the elemental and molecular features observed with such variations. CN violet band transitions with $\Delta\nu = 0$ were observed with greater magnitude among all but these peaks were intense in nitrogen atmosphere in comparison to others. The CN transitions of $\Delta\nu = +1$ and $\Delta\nu = -1$ were observed with low magnitude in RDX as well as TNT in argon atmosphere. Carbon peak at 247.82 nm was observed in all the nine spectra recorded (three samples and in three

Table 2
Description of elemental and molecular peaks obtained in three atmospheres for NTO, RDX, and TNT samples.

Species	Peaks (nm)	NTO			RDX			TNT		
		Air	N_2	Ar	Air	N_2	Ar	Air	N_2	Ar
C	247.82	*	*	*B	*	*	*B	*	*	*B
Ca	393.35, 396.83, 422.67	*	*	*	*	*	*	–	–	–
CN-($\Delta\nu = +1$)	359.02	*	*	*	*	*	*L	*	*	*L
CN-($\Delta\nu = 0$)	388.28, 387.07, 386.16, 385.40, 385.01	*	*B	*	*	*B	*	*	*B	*
CN-($\Delta\nu = -1$)	421.50, 419.63, 418.03, 416.78	*	*	*	*	*	*L	*	*	*
C_2-($\Delta\nu = +1$)	473.63, 471.50	–	–	–	–	–	–	*	*L	*
C_2-($\Delta\nu = 0$)	516.47	–	–	*L	–	–	*L	*	*	*B
Na	588.89, 589.50	*	*	*	*	*	*	–	–	–
H_α	656.2	*	*	*B	*	*	*	*	*	*B
O	777.2, 844.55	*B	*	*	*B	*	*	*B	*	*
N	821.50, 822.35	*	*	*	*	*	*	*	*	*
N	867.80, 868.80	*	*	*	*	*	*	*	*	*

* indicates the presence of peak, – indicates the absence of peak, L refers to peak presence with lower intensity (or buried in the noise), B refers to peak presence with higher intensity among three atmospheres.

atmospheres). When the spectra recorded with same gate delay and gate width were compared the intensity of carbon peak was observed to be higher in argon atmosphere which could, probably, be due to less carbon participation in the formation of CN molecule. The C_2 swan band transitions with $\Delta\nu = 0$ at 516.46 nm were observed in TNT for all atmospheres and were observed weakly in RDX and NTO in argon atmospheres. The other C_2 swan band transitions with $\Delta\nu = -1$ (471.50 nm, 473.63 nm) were observed only for TNT sample and it was strongly observed in argon atmosphere. As seen from the structures (shown in Table 1) of all three samples there are 7 C–C linkages in TNT whereas there are no C–C linkages in RDX and NTO. There are 5 C–N linkages in NTO, 6 C–N linkages in RDX and 3 C–N linkages in TNT. Post breakdown the molecules dissociate and form atoms and molecular radicals. The possible reason for C_2 being observed strongly in TNT sample is because TNT has more C–C native bonds and, therefore, the chances of C–C bonds breaking are higher compared to other molecules. The content of C atoms was also found to be higher in TNT. The H_α line at 656.2 nm was observed in all the spectra but was slightly enhanced in argon atmospheres. Oxygen triplet peaks at 777.2 nm and 844.5 were observed to be intense in air (availability of oxygen) but were observed with reduced intensity in nitrogen environment. Apart from main composition elements, peaks of some impurity elements like Ca in NTO and RDX spectra and Na doublet line in NTO spectra were also observed. Observed spectral features provide an insight of the phenomenon as to how the surrounding atmosphere affects the spectral features in LIBS data. Detailed analysis was performed using the ratios of spectral lines to gain better understanding about the dynamics from LIBS spectra of these samples.

3.2. Molecular and elemental ratio analysis

For a particular sample multiple LIBS spectra were recorded and comparison between their spectral intensity ratios of CN/C, CN/N, C_2/C, C_2/CN, O/N, C/O, C/N and H/N were ascertained. A total of 10 independent measurements were taken for each sample in all the three atmospheres. All spectra were recorded with a gate width of 800 ns and a delay time of 100 ns with respect to the input laser pulse. Bar charts for all the samples in different atmospheres are presented in Figs. 4 and 5 for all the above mentioned ratios. The bars represent 'mean' and error bars represent the 'standard deviation' of these 10 independent measurements. Fig. 4(a) represents the ratio of CN-388.28 nm to C-247.82 nm

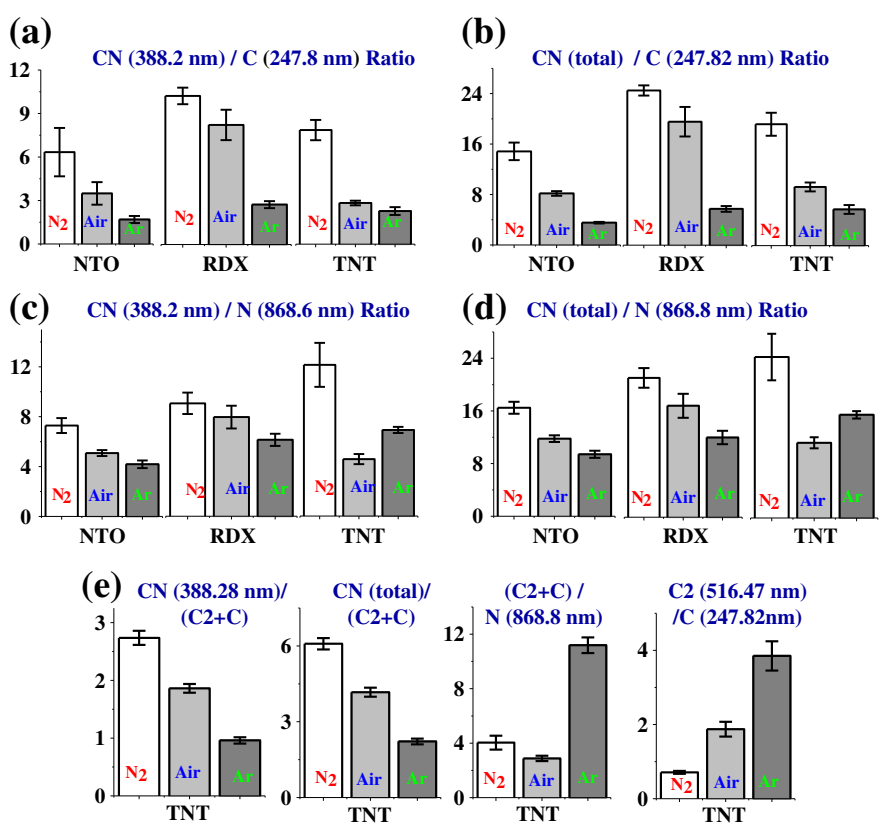

Fig. 4. Bar diagrams for intensity ratios of different species: (a) CN (388.28 nm)/C (247.8 nm), (b) CN (387.07 nm)/C (247.8 nm), (c) CN (388.28 nm)/N (868.8 nm), (d) CN (387.07)/N (868.8 nm) for NTO, RDX and TNT samples in three atmospheres (e) intensity ratios obtained for TNT with C_2 (516.47 nm). The error bars represent standard deviation of the ratios obtained from 10 independent measurements.

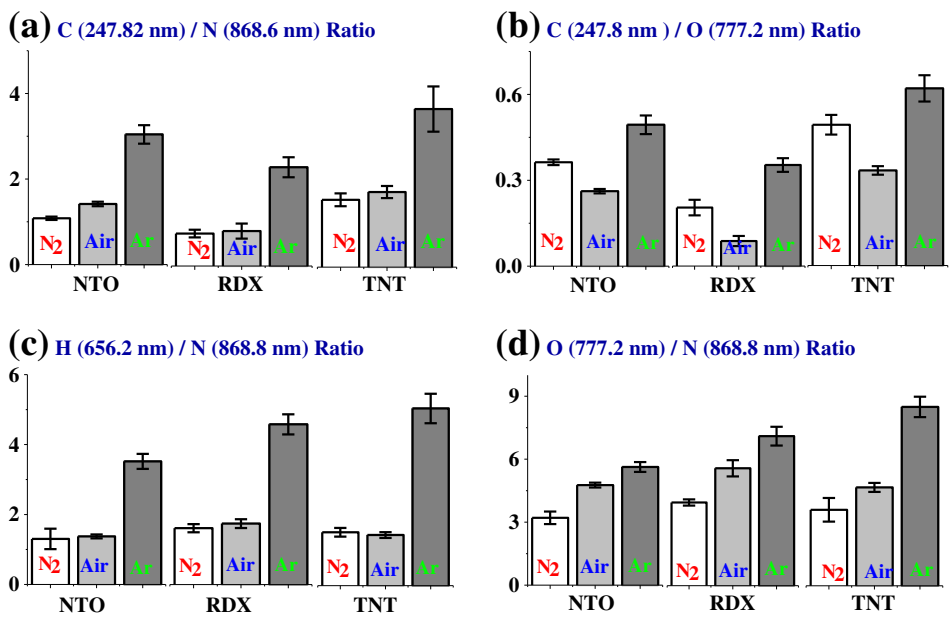

Fig. 5. Bar diagrams for elemental peaks intensity ratios of (a) C (247.82 nm)/O (777.2 nm), (b) C (247.82 nm)/N (868.8 nm), (c) H (656.2 nm)/N (656.2 nm) and (d) O (777.2 nm)/N (868.8 nm) for NTO, RDX and TNT samples in three different atmospheres. The error bars represent standard deviation of the ratios obtained from 10 independent measurements.

which was obtained for all the samples in three atmospheres. From NTO data the CN (388.2 nm)/C (247.80 nm) ratios measured [see Fig. 4(a)] had higher intensity in nitrogen atmosphere (6.3 ± 1.6) and was lower in air (3.4 ± 0.7) and lowest in argon (1.6 ± 0.2). Though the availability of carbon was from sample alone purging of the sample in different ambient gases [possessing different nitrogen percentages 100% for N_2 gas, 75% for air, and 0% for argon gas] led to the differences in the CN/C ratios. It is evident that elemental/molecular carbon in plasma reacts with the atmosphere surrounding it, which has decreasing nitrogen percentage (N_2 to argon), and is clearly reflected in the CN intensity. Similar trend was observed for all the three samples. This data clearly signifies that nitrogen present in ambient atmosphere played a major role in CN molecular formation.

Similarly Fig. 4(b) is plotted for CN (total)/C-247.8 nm, where CN (total) refers to addition of all three major CN peaks with $\Delta\nu = 0$ transitions. From Fig. 4(b) we conclude that in (a) nitrogen case: CN (total)/C (RDX) > CN (total)/C (TNT) > CN (total)/C (NTO) and (b) argon case: CN (total)/C (RDX) ≈ CN (total)/C (TNT) > CN (total)/C (NTO) while in (c) air case: CN (total)/C (RDX) > CN (total)/C (NTO) > CN (total)/C (TNT). We can explain these observations using the following arguments: (a) In the three samples studied NTO has less number of nitro-groups compared to others thereby suggesting lower CN formation with other parameters being the same; (b) in TNT we observed C_2 formation again suggesting formation of CN chances being lower; and (c) RDX has 3 nitro-groups and we also observed that C_2 formation was weaker therefore implying CN formation probability was indeed higher. Lucena et al. [34] studied different HEMs in air and helium (He) environments wherein they monitored CN/C_2 ratios and observed them to be stronger in air than in helium environment. They observed a corresponding increase in CN/C value with increase in number of nitro-groups present in the sample.

Fig. 4(c) and (d) corresponds to CN-388.2 nm/N-868.8 nm and CN (total)/N-868.8 nm ratios. CN/N ratios presented in Fig. 4(c) and (d) depict the variation observed similar to that of CN/C ratios in NTO and RDX samples. Since the percentage of nitrogen was decreasing from N_2 to argon atmospheres CN/N ratios were also observed to be decreasing for all the samples. In the case of TNT we observed that CN/N (N_2) > CN/N (argon) > CN/N (air). In argon purging we have observed intense C_2 emission in the TNT LIBS spectra. We believe that the atomic C was converted into C_2 and this could be the reason for the ratio being higher in argon compared to air. CN could be formed from C_2 and C species and, therefore, CN intensity was divided by total intensities of C_2 and C together. We have calculated additional ratios with C_2 + C peaks as shown in Fig. 4(e) between CN (388.2 nm)/[C_2 (516.47 nm) + C (247.8 nm)], CN (total)/[C_2 (516.47 nm) + C (247.8 nm)], [C_2 (516.47 nm) + C (247.8 nm)]/N (868.6 nm) and C_2 (516.47 nm)/C (247.82 nm) for TNT sample. The ratios of CN (388.2 nm)/(C_2 + C) and CN (total)/(C_2 + C) demonstrated a decreasing trend from nitrogen to argon atmosphere as the nitrogen content was decreasing. The (C_2 + C)/N and C_2/C ratios exhibited a high value in argon atmosphere signifying the formation of more C_2 species in argon. During argon purging the observed higher magnitude of C_2 could be due to the absence of surrounding nitrogen contributing towards the formation of CN radicals whereas in air/nitrogen atmospheres due to the presence of nitrogen CN formation could lead to depleted C_2 intensity.

The CN band formation in laser produced plasmas is mainly governed by a set of chemical reactions that take place within the plasma. The origin and temporal behavior of CN with the following set of reactions were studied extensively in laser produced plasmas from graphite and polymers as sources [36–44]. Ma et al. [45] and Babushok et al. [46] outlined few reactions involved in the formation C_2 species and are presented below:

$$C_{2(\mathrm{Plasma})} + N_{2(\mathrm{Surroundings\ or\ plasma})} \rightarrow 2CN_{(\mathrm{Plasma})} \quad (1)$$

$$2C_{(\mathrm{Plasma})} + N_{2(\mathrm{Surroundings\ or\ plasma})} \rightarrow 2CN_{(\mathrm{Plasma})} \quad (2)$$

$$C_{(\mathrm{Plasma})} + N_{2(\mathrm{Surroundings\ or\ plasma})} \rightarrow CN_{(\mathrm{Plasma})} + N_{(\mathrm{Plasma})} \quad (3)$$

$$C_{2(\mathrm{Plasma})} + N_{(\mathrm{Plasma})(\mathrm{gas})} \rightarrow CN_{(\mathrm{Plasma})(\mathrm{gas})} + C_{(\mathrm{Plasma})(\mathrm{gas})} \quad (4)$$

$$C_{(\mathrm{Plasma})(\mathrm{solid})} + N_{(\mathrm{Plasma})(\mathrm{gas})} \rightarrow CN_{(\mathrm{Plasma})(\mathrm{gas})} \quad (5)$$

$$CH_{(\mathrm{Plasma})} + CH_{(\mathrm{Plasma})} \rightarrow C_{2(\mathrm{plasma})} + H + H \quad (6)$$

$$C_{(\mathrm{Plasma})} + CH_{(\mathrm{Plasma})} \rightarrow C_{2(\mathrm{Plasma})} + H \quad (7)$$

$$C_{(\mathrm{Plasma})} + C_{(\mathrm{Plasma})} + M \rightarrow C_{2(\mathrm{Plasma})} + M. \quad (8)$$

The first three reactions refer to the formation of CN with nitrogen molecules. Reaction (1) occurs when C_2 reacts with N_2 and gets converted to CN molecule. This is the most prominent reaction for formation of CN in plasma [36,37]. Another possibility could be C_2 reacting with N_2^+ to give CN [41], but in our case we did not observe any N_2^+ features in the LIBS spectra and, therefore, we have not considered this reaction. In case of reactions (2) and (3), N_2 can react with atomic carbon to give CN molecule [41–43]. In all the above reactions the highest availability of N_2 for reactions will be from atmospheric air. Therefore, reactions (1) to (3) will be dominant when nitrogen surrounds the plasma and contribute strongly towards molecular CN formation. The other two reactions (4) and (5) refer to CN formation, when N reacts with C_2 and C species. The possibility of these reactions arises only from nitrogen presence as a sample constituent within the plasma. In our case we have used ~40 fs pulses to create the plasma. Consequently, the possibility of pulse interaction with the atmosphere is minimal and, therefore, chances of surrounding nitrogen breakdown and splitting into N atoms are less. This was evident from our previous work on LIBS studies of HEMs with fs and ns pulses [50] wherein we demonstrated that a number of nitrogen atomic peaks were less in fs LIBS spectra compared to ns LIBS spectra. The differences in the atmosphere will, consequently, affect the CN magnitude. In our experiments with nitrogen and air there will be abundant molecular N_2 surrounding the plasma and consequently these N_2 molecules will react with plasma strongly and form CN. In the case of argon atmosphere there is no presence of external nitrogen and the CN formation will take place with the N species present in the sample plasma only. In this situation the CN formation could be described by the reactions (4) and (5).

The elemental composition and the actual stoichiometric ratios of each sample are listed in Table 1. In all the three samples C/N and C/O elemental ratios [shown in Fig. 5(a) and (b)] were different in magnitude. The important conclusions from the data are (a) C/N and C/O ratios were higher in TNT than in RDX and NTO which is very well reflected in the ratio of their elemental composition seen from the formula (b) Both C/N and C/O were observed to be greater in magnitude in argon atmosphere since carbon is observed to be intense in argon spectra for all samples. Fig. 5(c) illustrates that in argon purging case H/N (TNT) > H/N (RDX) > H/N (NTO) which again replicates the sample composition. Hydrogen was observed to be very intense in argon atmosphere and hence the ratios evaluated will also be high in this atmosphere. Fig. 5(d) refers to O/N ratios for all samples in all atmospheres. The ratio was increasing in the order from NTO to TNT replicating the corresponding pristine sample composition.

3.3. Temporal studies of LIBS emission

Fig. 6(a)–(c) represents the intensity variation of C-247.8 nm peak for NTO, RDX and TNT samples. Carbon intensity was observed to be strong in argon atmosphere in comparison with nitrogen and argon. It also has longer decay time in argon (121 ± 16 ns) as compared to air (54 ± 3 ns) and nitrogen (43 ± 3 ns). The longer decay times could be a result of the lack of availability of nitrogen for depletion. In the presence of nitrogen, carbon reacts with it thereby depleting it leading to a faster decay rate. The decay constants of C and CN for all samples and in all three environments are listed in Table 3. Fig. 6(d)–(e) corresponds to temporal evolution of CN peak intensity for all three samples. The decay rate of CN followed CN (N_2) > CN (air) > CN (argon) for all the samples. In nitrogen and air as the plasma expands in time it interacts with surrounding nitrogen with an increase in CN molecular formation. Whereas in argon the CN will form with the help of nitrogen species available from the plasma alone which is comparatively less and, therefore, CN formation will be restricted and expected to decay faster.

The probability of CN species increases in air and nitrogen atmospheres with the presence of excess nitrogen whereas it is limited in argon. In the case of NTO and argon atmosphere we have observed C and CN peak intensities increase initially (up to 100 ns) and then decrease later with increasing delay time. From this we concluded that as C content increased/decreased CN content also increased/decreased accordingly following the reactions mentioned above. We observed the C peak intensity in nitrogen and air decayed very fast compared to argon case for all the samples. In the case of CN intensity the decay for NTO, RDX, and TNT was faster in argon than in nitrogen and air. Similar trend was also reported by Sovova et al. [48] who had investigated HEMs decay time in air and argon using ns pulses.

Fig. 7(a)–(c) represents the temporal variation in CN/C ratio for all samples. The spectra were collected with a 25 ns gate width and with a step size of 25 ns after an initial gate delay time of 80 ns with respect to the incident laser pulse. In all cases the available carbon amount is fixed since they are derived from the sample alone. The only difference being the change in nitrogen content in each situation. Fig. 7(a)

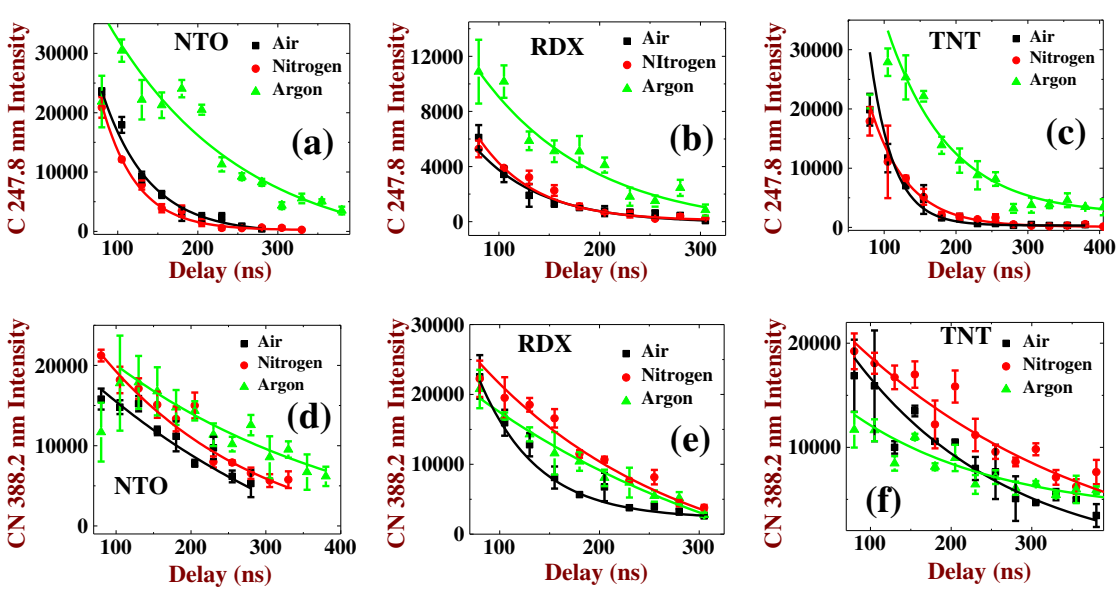

Fig. 6. Decay of C-247.82 nm peak in (a) NTO, (b) RDX and (c) TNT. Decay of CN-388.2 nm peak in (d) NTO, (e) RDX and (f) TNT. Spectra were recorded with a gate width of 25 ns and step size of 25 ns after an initial gate delay of 80 ns. The data points and error bars represent the mean and standard deviation, respectively, of the data obtained from three independent measurements. Solid lines are single exponential fits. Squares represent data in air, diamonds represent data in nitrogen, and triangles represent data in argon.

Table 3
Decay constants of C and CN peaks in different atmospheres.

Sample	Peak	Nitrogen (ns)	Air (ns)	Argon (ns)
NTO	C-247.82 nm	43 ± 3	54 ± 3	121 ± 16
	CN-388.2 nm	209 ± 70	172 ± 19	164 ± 46
RDX	C-247.82 nm	48 ± 4	48 ± 4	96 ± 28
	CN-388.20 nm	161 ± 22	107 ± 13	80 ± 15
TNT	C-247.82 nm	45 ± 3	65 ± 4	106 ± 9
	CN-388.20 nm	364 ± 25	181 ± 10	151 ± 42

illustrates that at initial time delays CN/C ratio for NTO increased slowly. After some time (~150 ns) the ratio increased sharply in nitrogen. But in argon atmosphere it continued increasing slowly. It was observed in all samples that the CN/C ratio increased gradually (up to ~150 ns) in all atmospheres. Near gate delay time of ~225 ns the CN/C ratio peaked in nitrogen atmosphere. The plasma starts expanding during certain period post laser pulse exit. In the process of expansion the plasma constituents react with the surrounding atmosphere. At these time scales the species present in the plasma will react with nitrogen present in the atmosphere. This could probably be the reason that CN/C ratio peaked near 225 ns. At initial time scales CN could form with its native radicals and with the chemical reaction occurring within the species present in the plasma only. At these time scales CN could form following reactions (4) and (5). As time progresses the plasma will expand and during this period the species present in the periphery of the plasma tries to interact with the surrounding atmosphere. The CN formation will boost as described by the reactions (1)–(3) with the N_2 gas present in surrounding atmosphere. Hence, at time scales of ~220–250 ns CN molecular formation could peak. The plasma with fs pulses lasted for ~400 ns beyond which we could not identify the signal since it was buried within the noise level. All the samples exhibited similar increment in the behavior of CN/C ratio in air and nitrogen atmospheres. But the CN/C ratio increment in argon atmosphere was very slow since there are no additional nitrogen atoms to interact with the plasma. The CN formation occurs with only the species present in the plasma.

Temporal variation of CN/N ratios is plotted in Fig. 8(a) to (c) for all samples. A similar trend was observed for the CN/N ratio also. Unlike CN/C ratio, which was observed to have a drastic increase around

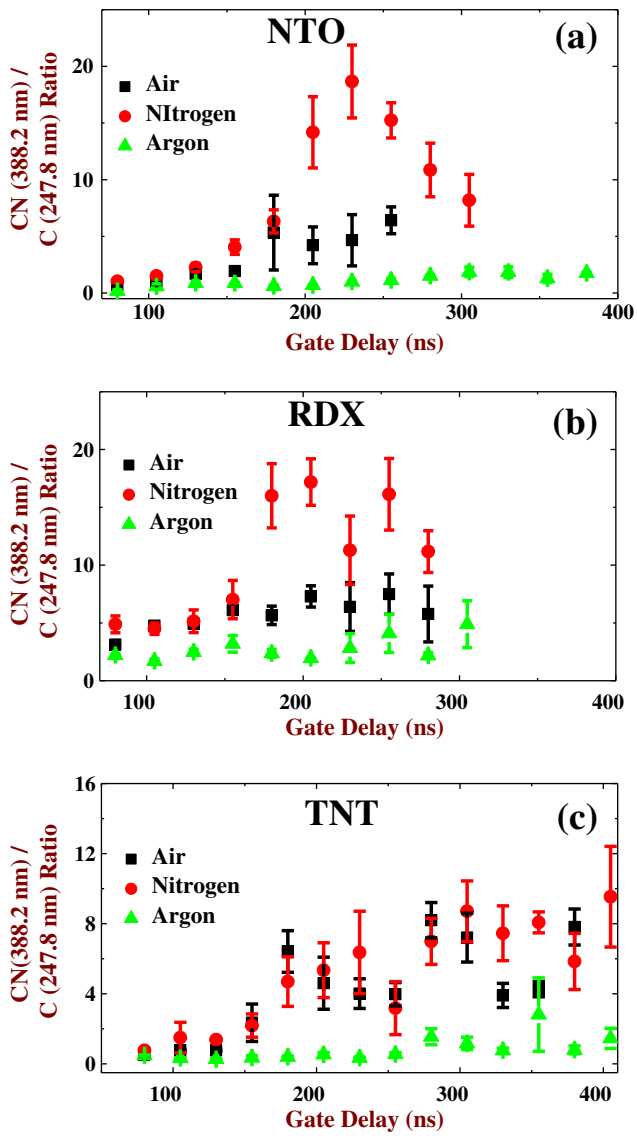

Fig. 7. Temporal evolution of CN (388.2 nm)/C (247.8 nm) in (a) NTO, (b) RDX and (c) TNT. Spectra were recorded with a gate width of 25 ns and step size of 25 ns after an initial gate delay of 80 ns. The data points and error bars represent the mean and standard deviation, respectively, of the data obtained from three independent measurements. Squares represent data in air, circles represent data in nitrogen, and triangles represent data in argon.

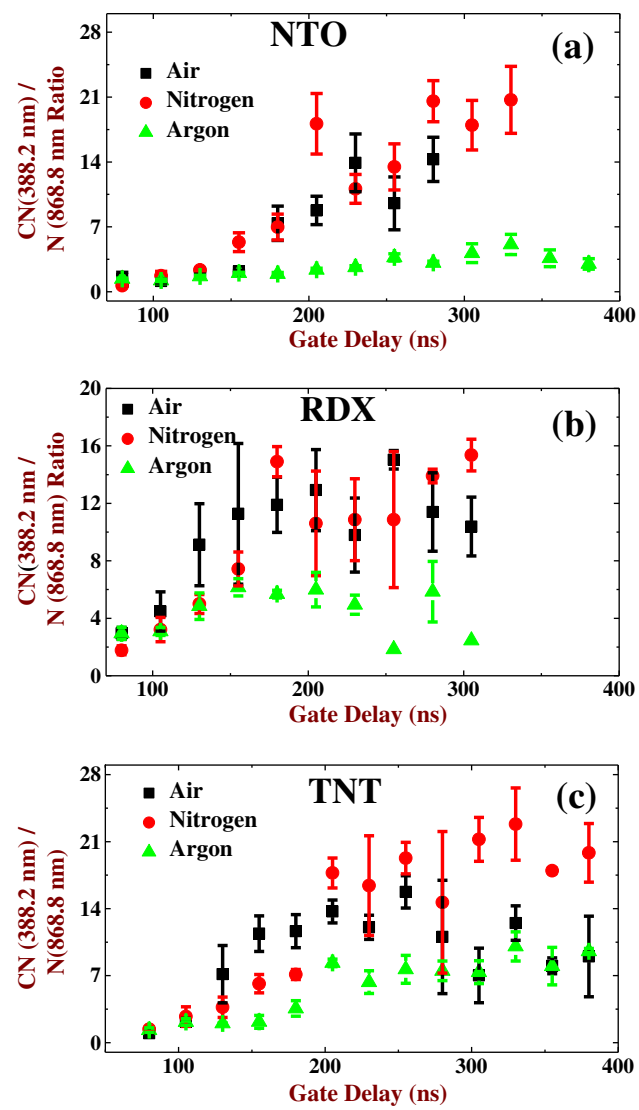

Fig. 8. Temporal evolution of CN (388.2 nm)/N (868.8 nm) in (a) NTO, (b) RDX and (c) TNT. Spectra were recorded with a gate width of 25 ns and step size of 25 ns after an initial gate delay of 80 ns. The data points and error bars represent the mean and standard deviation, respectively, of the data obtained from three independent measurements. Squares represent data in air, circles represent data in nitrogen, and triangles represent data in argon.

~150 ns, the sudden increase in CN/N was observed to start immediately after 100 ns. The increment in CN/N ratio was pronounced in air and nitrogen than in argon. This sudden increment in CN/N ratio could be attributed to the decrease in available nitrogen atoms which perish because of their participation in the reaction to form CN molecule. CN/C ratios of all the samples peaked in the 200–300 ns regime and subsequently came down beyond these time scales. Further detailed studies such as temporal studies of these samples in all three atmospheres in ns time domain are in progress to elucidate the exact mechanism(s) responsible for the increase/decrease of such ratios. The complete details of temporal variation of various molecular and atomic species could possibly provide us with mechanisms for detailed discrimination of HEMs.

4. Conclusions

Femtosecond LIBS spectra of NTO, RDX and TNT were obtained in different atmospheres and analyzed in detail. C-247.8 nm and H_α-656.2 nm peaks were observed to be intense in argon atmosphere. C_2-516.47 nm peak was observed to be very strong in argon atmosphere for TNT sample. The CN violet band for $\Delta\nu = 0$ transitions in the spectral range of 388–385 nm was observed to be strong in nitrogen and air atmospheres compared to argon. All possible reactions for CN formation were identified and discussed. Different molecular/elemental and elemental/elemental ratios were studied in various buffer gases. CN/C and CN/N ratios exhibited higher values in nitrogen and then decreased for data recorded in air atmosphere and further reduction was observed in the data recorded in argon atmosphere. Since the amount of surrounding nitrogen content reduces (nitrogen to air to argon atmospheres) the ratios were observed to be dwindling. The chemical reactions involved in the formation of CN, which are due to C_2 and C combining with molecular N_2 leading to the formation of CN, are dominant in nitrogen and air atmospheres because of the presence of large amount of nitrogen in their surroundings. In argon atmosphere the nitrogen species available in the plasma only will give rise to CN molecule implying lesser formation probability in this atmosphere. Temporal variation of C and CN peak intensity was studied in all three different atmospheres. The carbon peak decay was slower in argon than in other atmosphere for all samples whereas the CN peak decay was observed to be faster in argon atmosphere in comparison with other atmospheres. Temporal variations of CN/C and CN/N ratios were plotted for all samples in the three atmospheres. Around ~150 ns delay time there was a rise in the ratio observed in nitrogen and air atmospheres which emphasized that the CN molecular formation escalated due to the secondary reactions with the surrounding nitrogen.

Acknowledgments

Financial support from DRDO, India is gratefully acknowledged. The authors also acknowledge the samples provided by HEMRL, Pune, India and P. Ravi, ACRHEM.

References

[1] D.W. Hahn, N. Omenetto, Laser-induced breakdown spectroscopy (LIBS), part I: review of basic diagnostics and plasma particle interactions: still-challenging issues within the analytical plasma community, Appl. Spectrosc. 64 (2010) 335A–366A.
[2] D.W. Hahn, N. Omenetto, Laser-induced breakdown spectroscopy (LIBS), part II: review of Instrumental and methodological approaches to material analysis and applications to different fields, Appl. Spectrosc. 66 (2012) 347–419.
[3] M.A. Kumar, S. Sreedhar, S. Venugopal Rao, P. Prem Kiran, S.P. Tewari, G.M. Kumar, Laser induced breakdown spectroscopy-based investigation and classification of pharmaceutical tablets using multivariate chemometric analysis, Talanta 87 (2011) 53–59.
[4] N.C. Dingari, I. Barman, M.A. Kumar, S.P. Tewari, G.M. Kumar, Incorporation of support vector machines in the LIBS toolbox for sensitive and robust classification amidst unexpected sample and system variability, Anal. Chem. 84 (2012) 2686–2694.
[5] M.A. Kasem, R.E. Russo, M.A. Harith, Influence of biological degradation and environmental effects on the interpretation of archeological bone samples with laser-induced breakdown spectroscopy, J. Anal. At. Spectrom. 26 (2011) 1733–1739.
[6] V. Zorba, X. Mao, R.E. Russo, Ultrafast laser induced breakdown spectroscopy for high spatial resolution chemical analysis, Spectrochim. Acta Part B 66 (2011) 189–192.
[7] A. Assion, M. Wollenhaupt, I. Haag, F. Mayorov, C. Sarpe-tudoran, M. Winter, U. Kutschera, T. Baumert, T. Baumert, Femtosecond laser-induced-breakdown spectrometry for Ca^{2+} analysis of biological samples with high spatial resolution, Appl. Phys. B 77 (2003) 391–397.
[8] J.L. Gottfried, Discrimination of biological and chemical threat simulants in residue mixtures on multiple substrates, Anal. Bioanal. Chem. 400 (2011) 3289–3301.
[9] J.L. Gottfried, F.C. De Lucia Jr., C.A. Munson, A.W. Miziolek, Laser-induced breakdown spectroscopy for detection of explosives residues: a review of recent advances, challenges, and future prospects, Anal. Bioanal. Chem. 395 (2009) 283–300.
[10] M. Abdelhamid, F.J. Fortes, M.A. Harith, J.J. Laserna, Analysis of explosive residues in human fingerprints using optical catapulting-laser-induced breakdown spectroscopy, J. Anal. At. Spectrom. 26 (2011) 1445–1450.
[11] V. Lazic, A. Palucci, S. Jovicevic, M. Carpanese, Detection of explosives in traces by laser induced breakdown spectroscopy: differences from organic interferents and conditions for a correct classification, Spectrochim. Acta Part B 66 (2011) 644–655.
[12] B.N. Chichkov, C. Momma, S. Nolte, F. von Alvensleben, A. Tunnermann, Femtosecond, picosecond and nanosecond laser ablation of solids, Appl. Phys. A 63 (1996) 109–115.
[13] E.L. Gurevich, R. Hergenroeder, Femtosecond laser-induced breakdown spectroscopy: physics, applications, and perspectives, Appl. Spectrosc. 61 (2007) 233A–242A.
[14] Ph. Rohwetter, J. Yu, G. Me'jean, K. Stelmaszczyk, E. Salmon, J. Kasparian, J.-P. Wolf, L. Wöste, Remote LIBS with ultrashort pulses: characteristics in picosecond and femtosecond regimes, J. Anal. At. Spectrom. 19 (2004) 437–444.
[15] H.L. Xu, G. Méjean, W. Liu, Y. Kamali, J.F. Daigle, A. Azarm, P.T. Simard, P. Mathieu, G. Roy, J.R. Simard, S.L. Chin, Remote detection of similar biological materials using femtosecond filament-induced breakdown spectroscopy, Appl. Phys. B 87 (2007) 151–156.
[16] M. Baudelet, L. Guyon, J. Yu, J.-P. Wolf, T. Amodeo, W. Frejafon, P. Laloi, Femtosecond time-resolved laser-induced breakdown spectroscopy for detection and identification of bacteria: a comparison to the nanosecond regime, J. Appl. Phys. 99 (2006) 84701–84709.
[17] M. Baudelet, J. Yu, M. Bossu, J. Jovelet, J.-P. Wolf, T. Amodeo, E. Frejafon, P. Laloi, Discrimination of microbiological samples using femtosecond laser-induced breakdown spectroscopy, Appl. Phys. Lett. 89 (2006) 163903.
[18] D. Santos, R.E. Samad, L.C. Trevizan, A.Z. de Freitas, N.D. Vieira, F.J. Krug, Evaluation of femtosecond laser-induced breakdown spectroscopy for analysis of animal tissues, Appl. Spectrosc. 62 (2008) 1137–1143.
[19] E.J. Judge, G. Heck, E.B. Cerkez, R.J. Levis, Discrimination of composite graphite samples using remote filament-induced breakdown spectroscopy, Anal. Chem. 81 (2009) 2658–2663.
[20] S. Tzortzakis, D. Anglos, D. Gray, Ultraviolet laser filaments for remote laser-induced breakdown spectroscopy (LIBS) analysis: applications in cultural heritage monitoring, Opt. Lett. 1 (2006) 1139–1142.
[21] Y. Dikmelik, C. McEnnis, J.B. Spicer, Femtosecond and nanosecond laser-induced breakdown spectroscopy of trinitrotoluene, Opt. Express 16 (2008) 5332–5337.
[22] F.C. De Lucia, J.L. Gottfried, A.W. Miziolek, Evaluation of femtosecond laser-induced breakdown spectroscopy for explosive residue detection, Opt. Express 17 (2009) 419–425.
[23] M. Kotzagianni, S. Couris, Femtosecond laser induced breakdown for combustion diagnostics, Appl. Phys. Lett. 100 (2012) 264104.
[24] D.E. Roberts, A. du, J. Steyn Plessis, L.R. Botha, C.A. Strydom, I.J. van Rooyen, Femtosecond laser induced breakdown spectroscopy of silver within surrogate high temperature gas reactor fuel coated particles, Spectrochim. Acta Part B 65 (2010) 918–926.
[25] P. Ko, K.C. Hartig, J.P. McNutt, R.B.D. Schur, T.W. Jacomb-Hood, I. Jovanovic, Adaptive femtosecond laser-induced breakdown spectroscopy of uranium, Rev. Sci. Instrum. 84 (2013) 013104–013106.
[26] V. Zorba, J. Syzdek, X. Mao, R.E. Russo, R. Kostecki, Ultrafast laser induced breakdown spectroscopy of electrode/electrolyte interfaces, Appl. Phys. Lett. 100 (2012) 234101.
[27] X. Liu, D. Du, G. Mourou, Laser ablation and micromachining with ultrashort laser pulses, IEEE J. Quantum Electron. 33 (1997) 1706–1716.
[28] T. Gunaratne, M. Kangas, S. Singh, A. Gross, M. Dantus, Influence of bandwidth and phase shaping on laser induced breakdown spectroscopy with ultrashort laser pulses, Chem. Phys. Lett. 423 (2006) 197–201.
[29] K.C. Hartig, J.P. McNutt, P. Ko, T.W. Jacomb-Hood, I. Jovanovic, Pulse chirp effect in ultrafast laser-induced breakdown spectroscopy, J. Radiat. Nucl. Chem. (2012), http://dx.doi.org/10.1007/s10967-012-2038-x.
[30] K.L. Eland, D.N. Stratis, D.M. Gold, S.R. Goode, S.M. Angel, Energy dependence of emission intensity and temperature in a LIBS plasma using femtosecond excitation, Appl. Spectrosc. 55 (2001) 286–291.
[31] F.C. De Lucia Jr., J.L. Gottfried, C.A. Munson, A.W. Miziolek, Multivariate analysis of standoff laser-induced breakdown spectroscopy spectra for classification of explosive-containing residues, Appl. Opt. 47 (2008) G112–G122.
[32] F.C. De Lucia Jr., J.L. Gottfried, Characterization of a series of nitrogen-rich molecules using laser induced breakdown spectroscopy, Prop. Explos. Pyrotech. 35 (2010) 268–277.
[33] J.L. Gottfried, F.C. De Lucia Jr., C.A. Munson, A.W. Miziolek, Strategies for residue explosives detection using laser-induced breakdown spectroscopy, J. Anal. At. Spectrom. 23 (2008) 205–216.
[34] P. Lucena, A. Doña, L.M. Tobaria, J.J. Laserna, New challenges and insights in the detection and spectral identification of organic explosives by laser induced breakdown spectroscopy, Spectrochim. Acta Part B 66 (2011) 12–20.

[35] S. Grégoire, M. Boudinet, F. Pelascini, F. Surma, V. Detalle, Y. Holl, Laser-induced breakdown spectroscopy for polymer identification, Anal. Bioanal. Chem. 400 (2011) 3331–3340.
[36] L. St-Onge, R. Sing, S. Bechard, M. Sabsabi, Carbon emissions following 1.064 μm laser ablation of graphite and organic samples in ambient air, Appl. Phys. A 69 (1999) S913–S916.
[37] S.S. Harilal, R.C. Issac, C.V. Bindhu, P. Gopinath, V.P.N. Nampoori, C.P.G. Vallabhan, Time resolved study of CN band emission from plasma generated by laser irradiation of graphite, Spectrochim. Acta Part A 53 (1997) 1527–1536.
[38] K.F. Al-Shboul, S.S. Harilal, A. Hassanein, Spatio-temporal mapping of ablated species in ultrafast laser produced graphite plasma, Appl. Phys. Lett. 100 (2012) 221106.
[39] H.S. Park, S.H. Nam, S.M. Park, Time-resolved optical emission studies on the laser ablation of a graphite target: the effects of ambient gases, J. Appl. Phys. 97 (2005) 113103–113105.
[40] A. Kushwaha, R.K. Thareja, Dynamics of laser ablated plasma: formation of C_2 and CN, Appl. Opt. 47 (2008) G65–G71.
[41] J. Sun, H. Feng, J. Gan, Q. Li, K. Gao, N. Xu, Z.F. Ying, J.D. Wu, Reactive expansion of laser-induced boron/carbon plasma in ECR nitrogen plasma during the deposition of BCN films, Diam. Relat. Mater. 21 (2012) 66–72.
[42] D. Ding, P. Liang, J. Wu, N. Xu, Z. Ying, J. Sun, A comparative study of the enhancement of molecular emission in a spatially confined plume through optical emission spectroscopy and probe beam deflection measurements, Spectrochim. Acta Part B 79–80 (2013) 44–50, (2012).
[43] S. Grégoire, V. Motto-Ros, Q.L. Ma, W.Q. Lei, X.C. Wang, F. Pelascini, F. Surma, V. Detalle, J. Yu, Correlation between native bonds in a polymeric material and molecular emissions from the laser-induced plasma observed with space and time resolved imaging, Spectrochim. Acta Part B 74–75 (2012) 31–37.
[44] M. Dong, X. Mao, J.J. Gonzalez, J. Lu, R.E. Russo, Time resolved LIBS of atomic and molecular carbon form coal in air, argon and helium, J. Anal. At. Spectrom. 27 (2012) 2066–2075.
[45] Q. Ma, P.J. Dagdigian, Kinetic model of atomic and molecular emissions in laser-induced breakdown spectroscopy of organic compounds, Anal. Bioanal. Chem. 400 (2011) 3193–3205.
[46] P.J. Dagdigian, A. Khachatrian, V.I. Babushok, Kinetic model of C/H/N/O emissions in laser-induced breakdown spectroscopy of organic compounds, Appl. Opt. 49 (2010) C58–C66.
[47] V.I. Babushok, F.C. DeLucia Jr., P.J. Dagdigian, J.L. Gottfried, C.A. Munson, M.J. Nusca, A.W. Miziolek, Kinetic modeling study of the laser-induced plasma plume of cyclotrimethylenetrinitramine (RDX), Spectrochim. Acta Part B 62 (2007) 1321–1328.
[48] K. Sovova, K. Dryahina, P. Spanel, M. Kyncl, S. Civis, A study of the composition of the products of laser-induced breakdown of hexogen, octogen, pentrite and trinitrotoluene using selected ion flow tube mass spectrometry and UV–vis spectrometry, Analyst 135 (2010) 1106–1114.
[49] S. Rai, A.K. Rai, Characterization of organic materials by LIBS for exploration of correlation between molecular and elemental LIBS signals, AIP Adv. 1 (2011) 042103.
[50] S. Sreedhar, G. Manoj Kumar, M. Ashwin Kumar, P. Prem Kiran, Surya P. Tewari, S. Venugopal Rao, Femtosecond and nanosecond laser induced breakdown spectroscopic studies of NTO, HMX, and RDX, Spectrochim. Acta Part B 79–80 (2013) 31–38, (2012).